IEEE Photonics Journal
An IEEE Photonics Society Publication

Open Access

High Sensitivity of Temperature Sensor Based on Ultracompact Photonics Crystal Fibers

Volume 6, Number 6, December 2014

Hailiang Chen, Student Member, IEEE
Shuguang Li
Jianshe Li
Ying Han
Yidong Wu

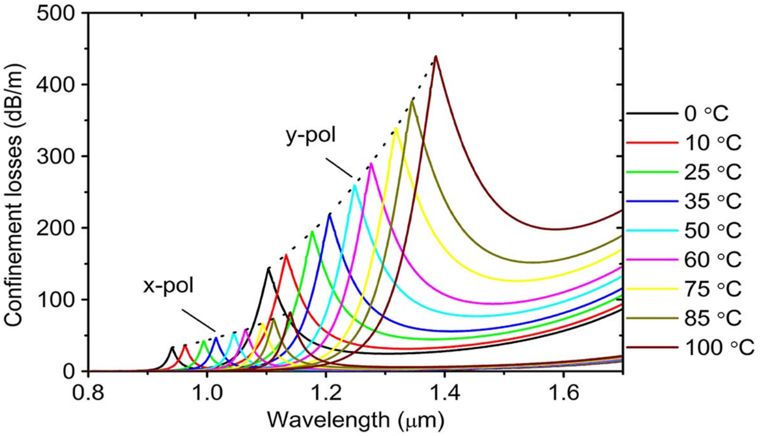

DOI: 10.1109/JPHOT.2014.2366157

High Sensitivity of Temperature Sensor Based on Ultracompact Photonics Crystal Fibers

Hailiang Chen, *Student Member, IEEE*, Shuguang Li, Jianshe Li, Ying Han, and Yidong Wu

State Key Laboratory of Metastable Materials Science and Technology, College of Science,
Yanshan University, Qinhuangdao 066004, China

DOI: 10.1109/JPHOT.2014.2366157

Manuscript received August 25, 2014; revised October 11, 2014; accepted October 15, 2014. Date of publication October 31, 2014; date of current version November 11, 2014. This work was supported in part by the National Natural Science Foundation of China under Grant 61178026 and in part by the Natural Science Foundation of Hebei Province, China, under Grant E2012203035. Corresponding author: S. Li (e-mail: shuguangli@ysu.edu.cn).

Abstract: A temperature sensor with high sensitivity based on ultracompact photonics crystal fibers is proposed and analyzed by the finite-element method. The temperature-sensitive materials are injected into one cladding air hole, which shows high confinement loss and works as a defect core. As the phase-matched condition is satisfied, the power in the transferring core couples to the defect core. The temperature sensitivity and figure of merit reach to 2.82 nm/°C, 0.105/°C and 1.99 nm/°C, 0.048/°C, for the *y*-polarized and *x*-polarized directions, respectively, which are one to two orders of magnitude better than other reported sensors. The performance characteristics can be further improved by optimizing the structure parameters and infilling materials.

Index Terms: Photonics crystal fibers, temperature sensitive materials, temperature sensor.

1. Introduction

The temperature sensor with compact structure and easy remote control is an important factor in the remote sensors and communication systems. Optical fibers, exhibiting high sensitivity, immunity to electromagnetic wave, corrosion resistance and easy remote control, have been utilized as the sensor medium in the past [1]–[3]. Grobnic [4] reported a sapphire fiber Bragg grating sensor with sensitivity of 25 pm/°C. Photonics crystal fibers (PCFs), benefit to its holey structure, are infiltrated with various functional materials to fabricate sensors. Lee [5] proposed a polymer filled hollow-core PCF temperature sensor showing high sensitivity of -1.7 nm/°C. Contrast to the difficult fusion splicing of polymer, it is relatively easier to fill the liquid into the air holes. Qiu [6] demonstrated an isopropanol-sealed PCF temperature sensor with sensitivity of -166 pm/°C. The side-polished microstructured optical fiber enhanced the effective area of the infilling material and a temperature sensitivity of 0.38 dB/°C is obtained [7]. Based on the intense surface plasmon resonance, the metal wires and films were injected into the air holes to get a high temperature sensitivity of 720 pm/°C [8].

In favor of high spectra acutance, various optical interferometers have been employed in sensing devices [9]–[11]. A high sensitive temperature sensors based on fiber loop mirror

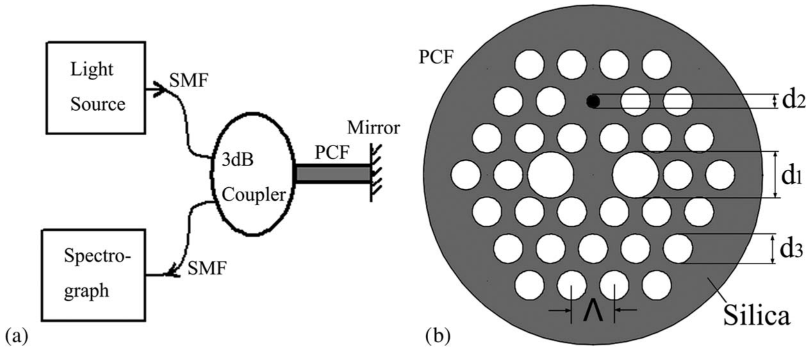

Fig. 1. (a) The schematic of temperature sensor system and (b) cross section of TSM-PCF. The black air hole is infiltrated with temperature sensitive materials.

interferometers have been reported with a high sensitivity of about 0.94 nm/°C [12]. Zhang [13] proposed a fiber optic extrinsic Fabry-Perot interferometer based on polymer-filled glass capillary with high sensitivity of 5.2 nm/°C. Limited to the free spectral range, however, the interferometers usually exhibit a narrow measurement range from 15 °C to 22 °C reported in [13].

In this paper, we designed a temperature sensor based on an ultra compact PCF. The temperature sensitive materials are supposed to be injected into one cladding air hole to form a defect core. As the phase matched condition is satisfied, the power in the transferring core couples to the defect core and the confinement losses increase remarkably. The defect core is labeled at the neighborhood of the transferring core and thus the couple can be complete. The designed temperature sensor avoiding transferring in high loss materials, showing ultra compact structure, low cost, high linearity, high sensitivity and figure of merit (FOM), are competitive for application in temperature measurement devices.

2. The Novel Design of Polarization Splitter

Fig. 1(a) shows the schematic of the designed temperature sensor system. The light source exports stable, continuous and broadband lights. The upper single mode fiber (SMF) connects the light source and the input port of the photonics crystal fiber which is infiltrated with temperature sensitive materials (TSM-PCF). The below SMF is utilized to connect the output port of the TSM-PCF and the spectrograph. A reflex mirror is located at the end of the TSM-PCF to increase the effective transferring distance. Fig. 1(b) depicts the cross section of the TSM-PCF. Two big air holes with diameters of d_1 are placed at the left and right of the core to achieve birefringence effect. The black air hole with diameters of d_2 is infiltrated with temperature sensitive materials. The rest air holes with diameters of d_3 are benefit to confine the power in the cores. The adjacent air holes pitch is labeled by Λ.

The background material of the TSM-PCF is fused silica and the dispersion relationship of which can be expressed by the Sellmeier equation [14]

$$n^2(\lambda, T) = (1.31552 + 6.90754 \times 10^{-6}T) + \frac{(0.788404 + 23.5835 \times 10^{-6}T)\lambda^2}{\lambda^2 - (0.0110199 + 0.584758 \times 10^{-6}T)} + \frac{(0.91316 + 0.548368 \times 10^{-6}T)\lambda^2}{\lambda^2 - 100} \quad (1)$$

where T is the temperature in Celsius, and λ is the free space wavelength in microns. Many liquids such as alcohol, methylbenzene, chloroform, and index-matching fluids exhibit high refractive index-temperature sensitive coefficient of about -4×10^{-4}/°C. In this paper, the refractive index of the temperature sensitive materials is designed as

$$n_{\mathrm{TSM}} = 1.37 - 4 \times 10^{-4}T \quad (2)$$

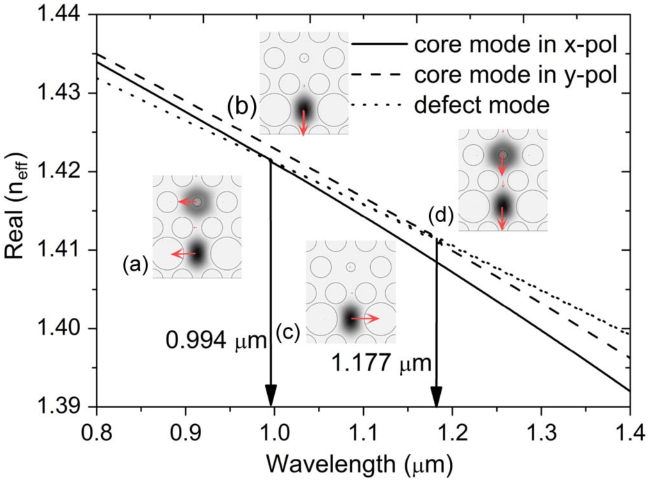

Fig. 2. Effective refractive indices of core modes and defect modes relying on wavelengths. The inserts show the electrical field profile at 0.994 μm in (a) the x-polarized direction and (b) the y-polarized direction and at 1.177 μm in (c) the x-polarized direction and (d) the y-polarized direction, respectively. The parameters are $d_1 = 2.2$ μm, $d_2 = 0.6$ μm, $d_3 = 1.4$ μm, $\Lambda = 2.0$ μm, and $T = 25$ °C.

where n_{TSM} is 1.37 at 0 °C. The actual measurement range is influenced by the freezing point and boiling point of the infilling liquid.

3. Simulation Results and Analysis

The FEM providing high accuracy and flexible triangular meshes was implemented to characterize the performance of the TSM-PCF. The scattering boundary conditions and a perfect matched layer were employed in the simulation process. As the refractive index of the temperature sensitive materials is less than silica, the temperature sensitive materials infilled air hole shows high confinement losses and works like a defect core. Fig. 2 shows the effective refractive indices of the core modes and defect modes. It is clear to see that the refractive indices of defect modes have intersections with the core modes at 0.994 μm in the x-polarized direction and 1.177 μm in the y-polarized direction. At the intersection point, the resonance appears and the energy couples between core modes and defect modes which can be clarified by the inserts in Fig. 2.

Fig. 3 demonstrates the confinement losses spectra of core modes and defect modes as a function of wavelength. At the intersection points, the confinement losses of core modes experience rapid increases and meanwhile the confinement losses of defect modes show fast decreases. It also should be noted that the confinement losses of core modes and defect modes are equal at phase matched points. It indicates that the imaginary parts of effective refractive indices are identical for core modes and defect modes. The couple between core modes and defect modes is complete which is benefit to obtain a high detection signal.

With the temperature increasing, the refractive index of the temperature sensitive material gets smaller. Thus, the refractive indices of defect modes become smaller, while the refractive indices of core modes have no significant variation. It results in a red shift of the phase matched points. Fig. 4 depicts the confinement losses spectra of core modes at different temperatures changing from 0 °C to 100 °C. The intensity of confinement losses at phase matched points increases as temperature increasing. It also should be pointed out that the couples between core modes and defect modes are always complete as temperatures changing from 0 °C to 100 °C.

Fig. 5 shows the resonant wavelengths as a function of temperature in x-polarized and y-polarized directions. The peak wavelengths increases linearly as temperature increasing from 0 °C to 100 °C, which is very important for application. The sensitivity of the designed temperature

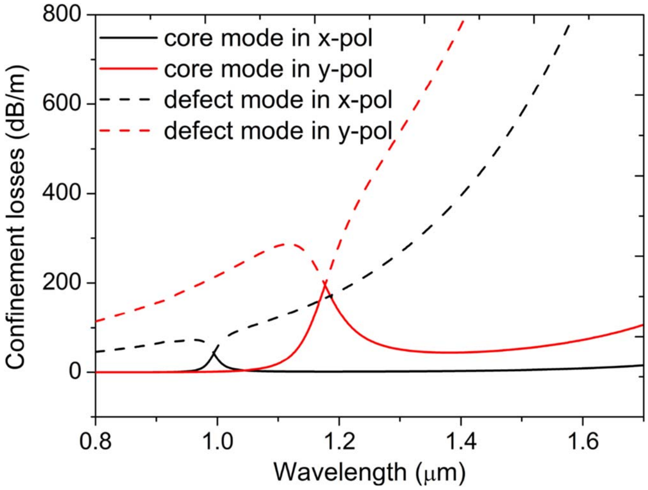

Fig. 3. Confinement losses spectra of core modes and defect modes relying on wavelengths.

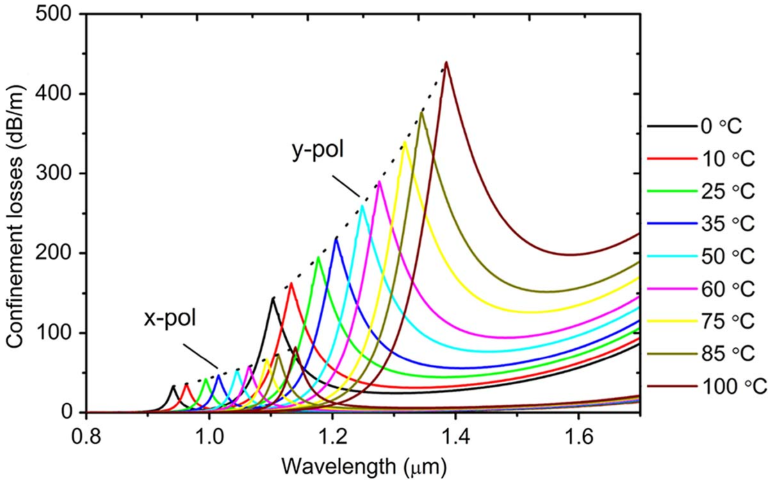

Fig. 4. Confinement losses spectra of core modes under different temperatures.

sensor is defined by $S = d\lambda_{\text{peak}}/dT$. It can be concluded from the fit lines that the sensitivity is 1.99 nm/°C for the x-polarized direction and 2.82 nm/°C for the y-polarized direction.

The spectra width and signal to noise ratio (SNR) both contribute to a better detection limit. This can be demonstrated by figure of merit (FOM). The FOM is defined by FOM=S/FWHM, where FWHM is the full width at half-maximum. Fig. 6 shows the FOM curves as a function of temperature. It reviews that FOM decreases linearly as the temperature increasing. This is mainly depended on the fact that the spectra width gets broadened as temperature increasing. The FOM is 0.0467 $^{\circ}\text{C}^{-1}$ for x-polarized direction and 0.10238 $^{\circ}\text{C}^{-1}$ for y-polarized direction at 0 °C.

The performance characteristics of the designed temperature sensor are influenced by the structure parameters of the PCF. It is well known that the mode's refractive index is mainly affected by the air holes of first ring [15]. As the diameters of d_2 increasing from 0.6 μm to 0.62 μm, the refractive index of the defect mode decreases. Meanwhile, the diameters of d_2 have no significant effect on the refractive indices of core modes. Thus, the phase matched points experience a red shift and the loss peaks move forward to the longer wavelengths as can be seen in Fig. 7. The decreasing of refractive index of defect mode also results in the increasing of resonant wavelengths displacement from 22 nm to 23 nm for the x-polarized

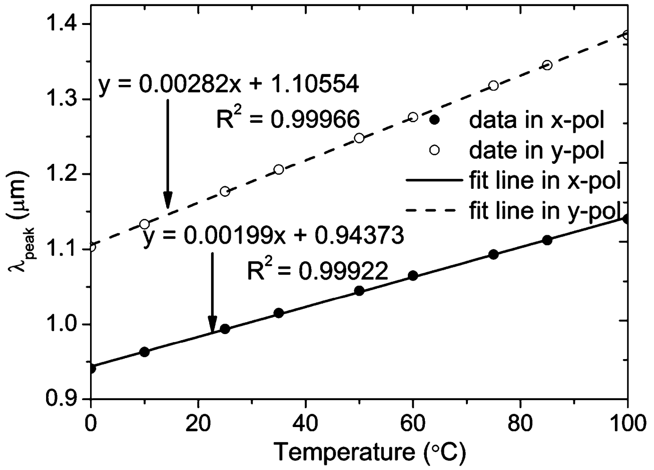

Fig. 5. The resonant wavelengths as a function of temperature in the x-polarized and y-polarized directions.

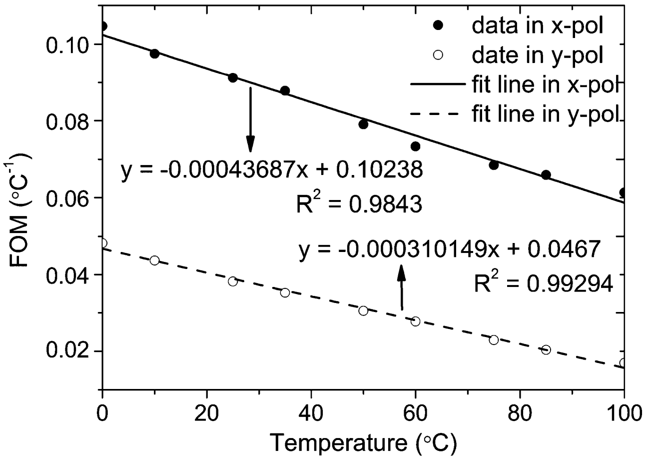

Fig. 6. The figures of merit as a function of temperature in the x-polarized and y-polarized directions.

direction and from 30 nm to 31 nm for the y-polarized direction, as temperature increasing from 0 °C to 10 °C. It indicates that the sensitivity of the temperature sensor can be improved by the increasing of d_2. The diameters of d_1 have vital influence on the refractive indices of core modes and faint influence on the refractive index of defect mode. The diameters of d_3 and adjacent air holes pitch simultaneously affect the refractive indices of core modes and defect mode. Thus, the resonant wavelength displacement and sensitivity can be further improved by adjusting the PCF structure parameters.

4. Conclusion

A high-sensitivity temperature sensor based on ultra compact PCFs is proposed. The temperature sensitive materials are injected into one cladding air hole and function as a defect core. The defect core is localized at the neighborhood of the transferring core to ensure that the couples between core modes and defect modes are complete. The sensitivity and FOM can reach to 1.99 nm/°C, 0.048/°C for the x-polarized direction and 2.82 nm/°C, 0.105/°C for the y-polarized direction, respectively. Both of the two polarized directions can be used to detect temperature

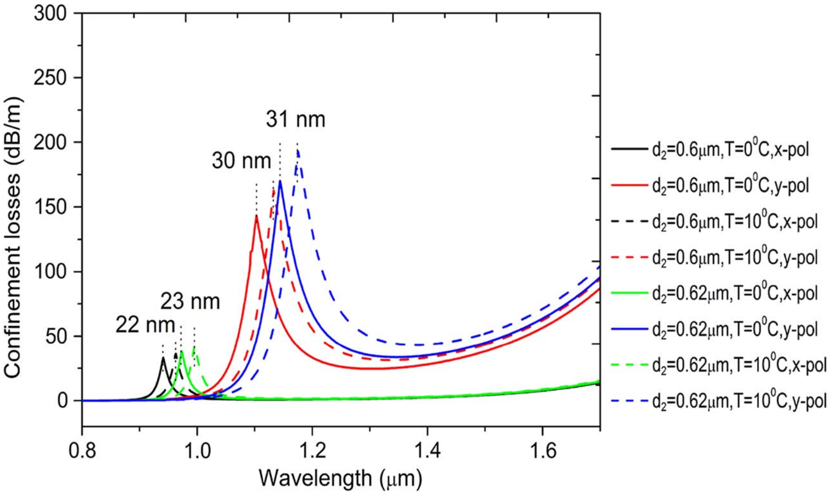

Fig. 7. Confinement losses spectra under different diameters of d_2.

and even self-correction. The performance characteristics can be further improved by optimizing the PCF structure parameters. The temperature sensitive materials with higher index-temperature coefficient also are very useful to enhance the performance characteristics. The designed temperature sensor showing perfect performance characteristics is suitable for the application in temperature measurement.

Acknowledgement

The authors wish to thank the anonymous reviewers for their valuable suggestions.

References

[1] S. K. Srivastava, R. Verma, and B. D. Gupta, "Surface plasmon resonance based fiber optic sensor for the detection of low water content in ethanol," *Sens. Actuators B, Chem.*, vol. 153, no. 1, pp. 194–198, Mar. 2011.

[2] P. S. Reddy *et al.*, "Method for enhancing and controlling temperature sensitivity of fiber Bragg grating sensor based on two bimetallic strips," *IEEE Photon. J.*, vol. 4, no. 3, pp. 1035–1041, Jun. 2012.

[3] P. Zu *et al.*, "Enhancement of the sensitivity of magneto-optical fiber sensor by magnifying the birefringence of magnetic fluid film with Loyt-Sagnac interferometer," *Sens. Actuators B, Chem.*, vol. 191, pp. 19–23, Feb. 2014.

[4] D. Grobnic, S. J. Mihailov, C. W. Smelser, and H. Ding, "Sapphire fiber Bragg grating sensor made using femtosecond laser radiation for ultrahigh temperature applications," *IEEE Photon. Technol. Lett.*, vol. 16, no. 11, pp. 2505–2507, Nov. 2004.

[5] C. L. Lee, L. H. Lee, H. E. Hwang, and J. M. Hsu, "Highly sensitive air-gap fiber Fabry–Pérot interferometers based on polymer-filled hollow core fibers," *IEEE Photon. Technol. Lett.*, vol. 24, no. 2, pp. 149–151, Jan. 2012.

[6] S. J. Qiu, Y. Chen, F. Xu, and Y. Q. Lu, "Temperature sensor based on an isopropanol-sealed photonic crystal fiber in-line interferometer with enhanced refractive index sensitivity," *Opt. Lett.*, vol. 37, no. 5, pp. 863–865, Mar. 2012.

[7] M. A. Franco, V. A. Serrao, and F. Sircilli, "Side-polished microstructured optical fiber for temperature sensor application," *IEEE Photon. Technol. Lett.*, vol. 19, no. 21, pp. 1738–1740, Nov. 2007.

[8] Y. Peng, J. Hou, Z. Huang, and Q. Lu, "Temperature sensor based on surface plasmon resonance within selectively coated photonic crystal fiber," *Appl. Opt.*, vol. 51, no. 26, pp. 6361–6367, Sep. 2012.

[9] P. Kozma, A. Hmori, S. Kurunczi, K. Cottier, and R. Horvath, "Grating coupled optical waveguide interferometer for label-free biosensing," *Sens. Actuators B, Chem.*, vol. 155, no. 2, pp. 446–450, Jul. 2011.

[10] W. Chen *et al.*, "Highly sensitive torsion sensor based on Sagnac interferometer using side-leakage photonic crystal fiber," *IEEE Photon. Technol. Lett.*, vol. 23, no. 21, pp. 1639–1641, Nov. 2011.

[11] K. Takahashi *et al.*, "Surface stress sensor using MEMS-based Fabry–Pérot interferometer for label-free biosensing," *Sens. Actuators B, Chem.*, vol. 188, pp. 393–399, Nov. 2013.

[12] Y. G. Liu *et al.*, "High-birefringence fiber loop mirrors and their applications as sensors," *Appl. Opt.*, vol. 44, no. 12, pp. 2382–2390, Apr. 2005.

[13] G. Zhang, M. Yang, and M. Wang, "Large temperature sensitivity of fiber-optic extrinsic Fabry–Pérot interferometer based on polymer-filled glass capillary," *Opt. Fiber Technol.*, vol. 19, no. 6, pp. 618–622, Dec. 2013.

[14] G. Ghosh, M. Endo, and T. Iwasaki, "Temperature-dependent Sellmeier coefficients and chromatic dispersions for some optical fiber glasses," *J. Lightw. Technol.*, vol. 12, no. 8, pp. 1338–1342, Aug. 1994.

[15] K. Saitoh and M. Koshiba, "Numerical modeling of photonic crystal fibers," *J. Lightw. Technol.*, vol. 23, no. 11, pp. 3580–3590, Nov. 2005.